Performance of Multibeam Echosounder Backscatter-Based Classification for Monitoring Sediment Distributions Using Multitemporal Large-Scale Ocean Data Sets

Snellen, Mirjam; Gaida, Timo; Koop, Leo; Alevizos, Evangelos; Simons, Dick

DOI
10.1109/JOE.2018.2791878

Publication date
2018

Document Version
Accepted author manuscript

Published in
IEEE Journal of Oceanic Engineering

Performance of multi-beam echo-sounder backscatter based classification for monitoring sediment distributions using multi-temporal large-scale ocean data sets

Snellen, M.[a,b], Gaida, T.C.[a], Koop, L.[a], Alevizos, E.[c], Simons, D.G.[a]

[a]Acoustics Group, Faculty of Aerospace Engineering, Delft University of Technology

[b]Deltares, Princetonlaan 6, 3584 CB Utrecht, The Netherlands

[c]GEOMAR Helmholtz Center for Ocean Research, 24148 Kiel, Germany

Abstract

Obtaining an overview of the spatial and temporal distribution of seabed sediments is of high interest for multiple research disciplines. Multi-beam echo-sounders allow for the mapping of seabed sediments with high area coverage. In this paper, the repeatability of acoustic classification derived from multi-beam echo-sounder backscatter is addressed. To this end, multi-beam echo-sounder backscatter data acquired on the Cleaver Bank (North Sea) during five different surveys is employed using two different classification methods, i.e., a method based on the principal component analyses and the Bayesian technique. Different vessels were used for the different surveys. The comparison of the classification results between the different surveys indicates good repeatability. This repeatability demonstrates the potential of using backscatter for long-term environmental monitoring. However, the use of different classification methods results in somewhat different classification maps. Monitoring, therefore, requires the consistent use of a single method. Furthermore, it is found that the statistical characteristics of backscatter is such that clustering algorithms are less suited to discern the number of sediment types present in the study area. The Bayesian technique accounting for backscatter statistics is therefore recommended. A strong positive correlation

between backscatter and median grain size for finer sediments (< 0.5 mm) using a frequency of 300 kHz is observed within the study area, but an ambiguity is found for sediments with median grain sizes > 0.5 mm. Consequently, for the situation considered a unique assignment of sediment type to acoustic class is not possible for these coarser sediments.

1. Introduction

Acoustic remote sensing with multi-beam echo-sounders (MBES) is extensively used for mapping the seafloor morphology because of the systems' capability to map large areas in relatively short time periods. However, capabilities of these acoustic underwater techniques extend beyond the determination of only the seafloor bathymetry. They also exhibit strong potential for classifying the seabed sediments by investigating the sediment backscatter strength that can be derived from the intensities of the received echo. The backscatter strength is physically attributed to seabed properties such as sediment bulk density, seafloor roughness, volume heterogeneity, discrete scatterers and sediment layering [1] [2] [3]. The contribution of each factor to the backscatter strength is dependent on the complexity of the seabed, acoustic frequency and angle of incidence [3]. Several regional studies have revealed a relationship of backscatter to sediment properties such as median grain size [4] [5], grain size distribution [6] [7] [8], or shell or gravel content [9] for a specific study area and frequency. However, other studies have shown that in diverse environments additional factors such as benthic fauna [10] [11], activity of benthic organisms [12], sediment compaction [13] or natural hydrocarbons [14] [15] may influence the backscatter strength of the seafloor as well.

In general, classification methods employing measured backscatter data can be divided into model-based and image-based methods [16]. Model-based methods are attributed to techniques that perform inversion based on physical backscatter models either to exploit the measured backscatter strength directly [17] or the angular backscatter response [18] to invert

for sediment properties (e.g. mean grain size, roughness spectrum, volume scattering coefficient). Image-based methods are based on statistical relationships and patterns within the backscatter data [19] [20]. Whereas model-based methods require accurate models for predicting the backscatter strength and well-calibrated systems for measuring backscatter strength [3] [21], image-based techniques are also applicable to relative backscatter values from poorly or uncalibrated systems.

Reference [22] gives a review of various strategies and methods employing acoustic remote sensing techniques including SBES, SSS and MBES to produce sediment or habitat maps. They present 147 studies utilizing acoustic survey techniques published during the last two decades. This is a good indicator for the intensive research already carried out and the still ongoing development in the scientific field of seafloor classification. Among others, they classify image-based methods in objective/subjective and supervised/unsupervised strategies. The classification methods applied in this study, i.e. the Principal Component Analysis (PCA) and Bayesian technique, can be referred to as image-based, objective and unsupervised strategies. The PCA and Bayesian techniques have been successfully applied to MBES backscatter in several studies [4], [20], [23], [24].

Using the full MBES acoustic data content gives the opportunity for the development of marine-landscape maps displaying topography and the seabed sediment spatial distribution simultaneously. Because of physical and biological, as well as anthropogenic processes, the seafloor is a time-varying environment. Monitoring this dynamic environment requires good repeatability of the methods for seabed sediment classification. That means the data gathering, processing, and interpretation must lead to equal results for different measurement campaigns if the environment does not change. However, regarding the use of MBES measurements for sediment classification, repeatability of the results is a topic of concern. Reference [21] points out the acoustic-instrument stability, settings, processing algorithms, range, environmental

76 conditions, and survey methods as critical factors influencing the classification results, and
77 consequently, affect repeatability. Therefore, there is a strong demand from the MBES
78 backscatter community for data quality control, standardised acquisition and processing steps
79 as well as detailed documentation of the processing chain within MBES systems [25]. In the
80 research field of seafloor classification with MBES the ultimate goal is to generate consistent
81 and repeatable results within the same area under the same settings from backscatter data
82 acquired by differing MBES systems or analysed by different processing procedures [26].

83 The goal of this paper is to apply two different classification methods to MBES backscatter
84 data acquired on different vessels during different surveys carried out in various time periods
85 and to investigate the repeatability and agreement of the resulting sediment maps. To
86 accomplish this goal, the Bayesian approach and PCA in conjunction with k-means clustering
87 approach are applied to backscatter data acquired on the Dutch vessels Zirfaea and Arca in the
88 Cleaver Bank area in the time period from 2013 to 2015. This study site consists of a
89 significant number of sediment types, and intersecting survey tracks within the source data of
90 this study allow for the investigation of the repeatability of the results. The classification
91 results are compared to ground truth data to investigate the relationship between acoustic
92 classes and sediment properties. The spatial resolution capabilities of the classification
93 methods are additionally addressed to illustrate the state of the art of methods for MBES
94 seabed sediment classification.

95 This paper is organized as follows. In Section 2 the study area and the data are described.
96 Section 3 gives an overview of the two classification methodologies that are applied. Then,
97 Section 4 presents the results from applying the classification algorithms along with
98 considerations such as the number of sediment classes that can be discerned. Section 5 is a
99 discussion of the results, addressing the repeatability of the classification, the spatial

100 resolution, the issue of assigning sediment type to the acoustic classes, as well as a discussion
101 on the ambiguity for large grain sizes. Finally, in Section 6 the conclusions are presented.

102 2. Study area and data

103 The Cleaver Bank area is located 160 km north-west from Den Helder in the Dutch North Sea
104 (Fig. 1) and is part of the nature protection areas in the territory of the European Union. The
105 area was formed as a terminal moraine of a glacier during the Weichselian Ice Age. The water
106 depth mainly varies between 25 m and 50 m, but is divided from north-west to south-east by a
107 70 m deep channel called the Botney cut (Fig. 1). The Cleaver Bank extends over an area of
108 about 900 km^2 and is the largest area within the Dutch North Sea with coarse sediments [27].
109 In comparison to the mostly sandy areas of the Dutch seafloor the Cleaver Bank consists of
110 the entire grain size spectrum from mud to gravel with isolated boulders. The diverse geology
111 of the Cleaver Bank seafloor is a result of the Weichselian Ice Age and is relatively well
112 preserved due to the combination of the sufficiently large depth and the rocky bottom which
113 reduces the erosive influence of waves [28].

114 The MBES data considered in this work were acquired in the Cleaver Bank area during five
115 surveys carried out within the period from November 2013 to February 2015. The entire
116 survey area is 57 km in the north-south direction and 30 km in the west-east direction. In
117 general, the survey lines are separated by approximately 1500 m except a few lines spaced
118 closer together, overlapping lines, and several cross lines (Fig. 1). The swath width ranges
119 from 90 m to 180 m depending on the water depth. Two different vessels, the Zirfaea and
120 Arca, were both equipped with a Kongsberg EM3002 single head MBES sonar system using a
121 central frequency of 300 kHz. The transmit and receive beam width are both 1.5° for nadir
122 angles. The transmitted pulse length was set to 150 μs and the number of beams were 258
123 along the entire swath. These parameters were kept constant during each survey. Furthermore,

124 the same transmitted source level, receiver gain and time-varying gain were applied during the
125 different surveys. The acquired MBES data were corrected for roll, pitch and heave.
126 Depending on the different environmental conditions, the water absorption coefficient was
127 calculated for each survey individually. The MBES data were also corrected for tidal effects.

128 To obtain a relatively good approximation of the backscatter strength from the received
129 acoustic echo several steps are carried out within the Kongsberg MBES. The system corrects
130 in real time for transmission loss (attenuation and geometrical spreading), insonified area as
131 well as for transmission and reception beam pattern [29]. However, the real-time correction
132 for the insonified area assumes a flat seafloor. Therefore, the backscatter data is corrected for
133 the seafloor bathymetry slope in post processing to obtain the true insonified area [30].
134 However, some of the real-time correction performed by Kongsberg still includes
135 simplification of the marine environment (e.g. constant absorption coefficient, flat seafloor
136 assumption for reception process) which might affect the true backscatter strength [26]. In
137 addition, a MBES calibration that would account for the alteration of sonar transducers'
138 sensitivities or deviation of the system configuration from the manufacturer specification was
139 not performed. Taking these factors into account, strictly speaking, the employed acoustic
140 data represent a relative rather than absolute backscatter strength because the data might still
141 not be entirely independent of the MBES configuration or environmental impacts. Therefore,
142 we are using the term backscatter data or backscatter values in this paper instead of
143 backscatter strength.

144 For validation and assignment of sediment type to acoustic class, 104 Hamon and Van Veen
145 grab samples were taken during four different surveys in 2000, 2013, 2014 and 2015 (Fig. 1).
146 The grab samples were sieved to separate the gravel and shell fragments from the sand and
147 mud fraction. The latter part was analysed by laser-diffraction granulometry. The percentage
148 of the different grains was used to classify the grab samples after the Folk scheme [30].

149 Almost no shell fragments or other biological particles were found to be present in the grab
150 samples. Because the seafloor dynamics of the Cleaver bank are low, the grab samples from
151 2000 are considered to be valid.

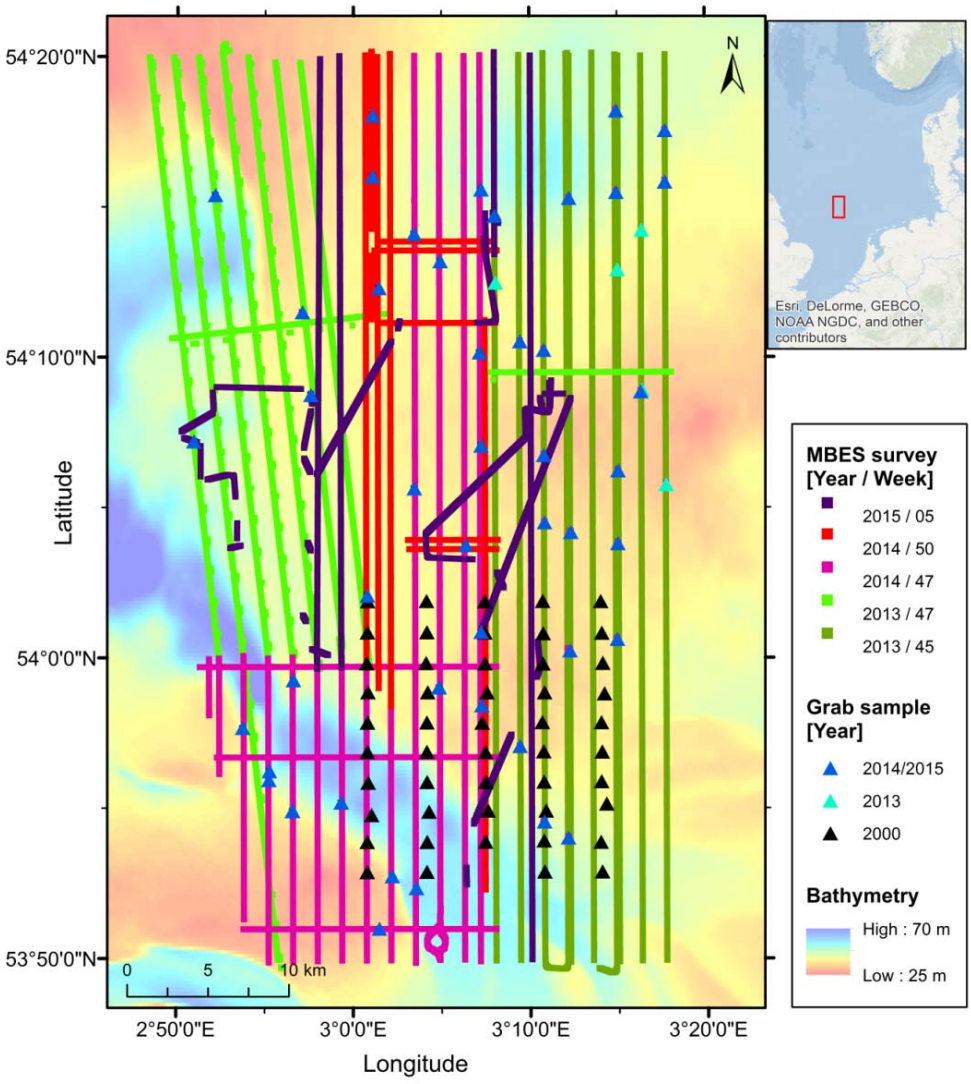

152

153 **Fig. 1 . MBES tracks of five different surveys carried out from 2013 to 2015 are plotted over the bathymetry of the**
154 **Cleaver Bank. Bathymetry is received from EMODnet [31]. Grab samples taken in the years 2000 and 2013 to 2015**
155 **are denoted by triangles.**

156 ## 3. Classification methods

157 In this study two unsupervised sediment classification methods, the Bayesian technique and
158 PCA in conjunction with k-means clustering, are applied to the MBES data of the Cleaver

Bank. The Bayesian technique for seafloor classification was developed in [23] where also a detailed theory description is given. It has since been used in [4], [20], [24], and [32] among others. This section provides a brief overview of the basic concepts and the relevant processing steps to generate the sediment maps of the Cleaver Bank. The theory of PCA was first introduced by [33] [34]. Today many different variations of PCA exist which are adapted depending on the application purposes. A very detailed explanation of the application to MBES data is given by [20].

3.1 Bayesian technique

Assuming that a beam footprint contains a large number of scatter pixels, based on the central limit theorem, the backscatter strength per beam footprint can be assumed to be Gaussian distributed [23]. A scatter pixel here is the instantaneously insonified area of the sea floor within a beam footprint of the MBES. Given a constant frequency and angle of incidence, the backscatter strength is dependent on the seabed properties. It follows that if a survey area has a total of m different sediment types, with specific seabed properties, then the backscatter histogram from a selected oblique beam of the echo-sounder should be represented by a combination of m Gaussian distributions. Consequently, the model for the histogram of measured backscatter values per beam can be written as

$$f(y_j|\mathbf{x}) = \sum_{k=1}^{m} c_k \exp\left(-\frac{(y_j - \bar{y}_k)^2}{2\sigma_{y_k}^2}\right) \quad (1)$$

where $f(y_j|\mathbf{x})$ is the value of the model at backscatter value y_j, and $\mathbf{x}$ is the vector containing the unknown parameters, $\mathbf{x} = (\bar{y}_1, \dots, \bar{y}_m, \sigma_{y_1}, \dots \sigma_{y_m}, c_1, \dots, c_m)$, i.e. the means $\bar{y}_k$, standard deviations σ_{y_k} and coefficients c_k of the Gaussian distributions that represent

each seafloor type. By fitting the above model to the measured histogram all unknowns are determined.

With a new data set, one may not know how many sediment types there are in the survey area. By conducting a χ^2 goodness of fit test, the optimal number of Gaussians m can be determined where χ^2 is defined as:

$$\chi^2 = \sum_{j=1}^{M} \frac{\left(n_j - f\left(y_j|\mathbf{x}\right)\right)^2}{\sigma_j^2} \tag{2}$$

Here the n_j denote the number of measurements per bin (in our case the bin size is 0.5 dB) of the previously mentioned histogram and M is the total number of bins in the histogram. For the n_j a Poisson-distribution is postulated[1]. The variances σ_j^2 are thus equal to n_j. The goodness of fit statistic is χ^2 distributed with $v = M - 3m$ degrees of freedom. The goodness-of-fit criterion is then further defined as the reduced-χ^2 statistic ($\chi_v^2 = \chi^2/v$) having a value close to one [35, pp. 68, 195 - 197]. The value of m for which a further increase of m does not generate a better fit of the model to the histogram, as quantified by the reduced-χ^2 measure, is taken to be the number of seafloor types that can be discriminated in the survey area based on the backscatter data.

For the classification, the Bayes decision rule is applied, where there are m states or hypotheses. These hypotheses correspond to the m seafloor types present in the surveyed area. From Bayes and assuming all hypothesis to be equally likely, it is found that the intersections

[1] The requirements for an event being Poisson distributed are that (1.) E is the number of times the event in question occurs in an interval of time or space. (2.) $E \in 0 \cup \mathbb{N}$ (3.) The events are independent. (4.) The probability of the event occurring does not vary with time. (5.) Two events cannot occur at the same time. (6.) The probability of an event in a small interval is proportional to the length of the interval.

of the m Gaussian PDFs provide the m non-overlapping backscatter acceptance regions, corresponding to the m seafloor types.

3.2 Principal component analysis and k-means clustering

PCA is a statistical method to reduce the complexity of a dataset while preserving most of the information content. This is achieved by transforming the original data set consisting of p (potentially) correlated variables to a new data set of $\ell = 1, 2, \ldots, p$ uncorrelated variables Y_ℓ, the so-called principal components (PCs). Each PC can be seen to account for a part of the variation in the feature values of the original data set. Therefore, the size of the original data set can be reduced by considering only the PCs representing a significant portion of the data variability.

The n measurements of the p variables, often called features, are summarized in an $(n \times p)$ data matrix. To account for different magnitudes of the features, the data are standardized, where for each feature the mean is determined and subtracted from the measurements of that feature. In addition, the features are divided by their standard deviation. The matrix **F** contains these standardized measurements. The first step of PCA is the calculation of the covariance matrix of **F** as

$$\mathbf{R} = \frac{1}{n}\sum_{j=1}^{n} \mathbf{F}_j{}^T \mathbf{F}_j \tag{3}$$

with $\mathbf{F}_j$ the j^{th} row of the matrix **F.** Superscript T denotes the transpose. The second step is to determine the eigenvectors and the corresponding eigenvalues of **R** by solving

$$\mathbf{RA} = \mathbf{A\Lambda} \tag{4}$$

with $\mathbf{A}$ the (p x p) eigenvector matrix whose columns are the eigenvectors $\boldsymbol{a}_\ell$ and $\mathbf{\Lambda}$ the (p x p) eigenvalue matrix where the diagonal elements are the corresponding eigenvalues λ_ℓ of the covariance matrix $\mathbf{R}$.

The obtained eigenvector matrix $\mathbf{A}$ is used to transform the original data set $\mathbf{F}$ into the new data set consisting of the PCs. Thus, the original measurements $\mathbf{F}_j$ can be written as a sum over the eigenvectors, i.e.,

$$\mathbf{F}_j = \mathbf{Y}_j\mathbf{A}^{\mathrm{T}} \tag{5}$$

with the coefficients for the eigenvectors contained in the row vector $\mathbf{Y}_j$ of matrix $\mathbf{Y}$. Thus, one finds

$$\mathbf{Y}_j = \mathbf{F}_j(\mathbf{A}^{\mathrm{T}})^{-1} \tag{6}$$

where the full matrix $\mathbf{Y}$ is of size (n x p), as is the original matrix $\mathbf{F}$, and contains for the n measurements the p coefficients for the eigenvectors. In general, although different definitions exist, the ℓ^{th} column $\boldsymbol{Y}_\ell$ of $\mathbf{Y}$ is considered as the ℓ^{th} PC, given by

$$\mathbf{Y}_\ell = \mathbf{F}\boldsymbol{a}_\ell \tag{7}$$

The amount of variability in the original data set which is accounted for by the PC $\mathbf{Y}_\ell$ is quantified by the eigenvalue λ_ℓ. Based on these eigenvalues a subset of PCs can be selected that represent the majority of the variations in the measurements. For this work, the subset was selected such that 70% to 90 % of the data variability is accounted for. These PCs are then supplied to the k-means algorithm to group the PCs into different clusters [36].

The k-means clustering algorithm aims to assign the n data points for each of the PCs into k predefined clusters S_i $(i = 1,\ldots,k)$. Thereby the sum of the squared Euclidean distance between the data points and the average of all data points within the cluster, i.e., the so-called cluster centroid, is minimised. The minimisation problem is thus

$$min \sum_{i=1}^{k} \sum_{x_s \epsilon S_i} |x_s - c_i|^2 \quad (8)$$

where x_s is a data point within the cluster i and c_i is the cluster centroid of the cluster i.

The application of the k-means algorithm to a dataset requires a predefined number of clusters k. However, the estimation of how many clusters to use is a well-known issue in unsupervised classification methods [37] and is in general the most subjective part of a cluster analysis. In this study three different statistical methods are applied to the MBES backscatter dataset to determine the number of clusters.

The statistical methods are applied to the output of the clustering techniques using varying numbers of clusters. The first method, the gap statistic, was proposed by [38]. This method calculates the overall within-cluster variance of the dataset and compares this value to an expected value calculated for an appropriate reference distribution. The estimated number of clusters is defined where the logarithmic overall within-cluster variance value is minimized. A detailed mathematical description is found in [38]. The second method, the Silhouette statistic, is developed by [39]. The average distance of the observations within the clusters and the average distance of the observations to the data points in the nearest clusters is calculated for each number of clusters. The values are called the Silhouette coefficients. The optimal number of clusters is selected where the Silhouette coefficient is maximized. Finally, the David-Bouldin criterion is also used in this study [40]. This method examines the ratio of the

252 within-cluster distance and between-cluster distance. The optimal clustering solution is
253 represented via the smallest David-Bouldin index. In [38], the performance of several cluster
254 number estimation methods including the gap statistic and the Silhouette coefficient was
255 investigated. That study demonstrated that the gap-statistic performs most efficiently.

256 # 4. Results

257 In this section, the results of the two classification methods are presented. Both methods
258 employ the MBES backscatter data for the classification of the seafloor.

259 ## 4.1 Bayesian method

260 For the application of the Bayesian method we use receiving beams between 20° and 60°. The
261 beams between nadir and 20° are not used because firstly, there are too few scatter pixels to
262 meet the central limit theorem requirement and secondly, these beams are less sensitive to
263 sediment properties (e.g. roughness) variation than the outer beams [41]. Often receive beams
264 beyond 60° can also be used for classification but for the data considered here, those beams
265 tended to be too noisy to yield reasonable results.

266 The estimation of the optimal number of classes is a well-known issue in unsupervised
267 classification methods [37]. For the Bayes method, however, a statistically sound approach is
268 available. Here, the curve fitting procedure as described in Section 3.1 is executed for
269 increasing numbers of sediment types m. The number of sediment types present in the area is
270 taken as that value of m for which a further increase in m does not result in a further
271 improvement of the fit. The goodness of fit is quantified through the reduced χ_ν^2 statistic. For
272 the Cleaver Bank data, it is found that a maximum of seven sediment types can be
273 discriminated based on the available backscatter data. Fig. 2 shows an example of the χ_ν^2
274 statistic for an increasing number of Gaussians and for the 48° beam from nadir, for both the

2013 and 2014/2015 data, as well as the two sides (starboard and port). It is seen that for the 2013 data as well as for side 2 of the 2014 and 2015 data the use of 7 Gaussians provides a very good fit between modelled and measured histogram, with the χ_ν^2 statistic being close to 1. An example, indicating that sometimes the χ_ν^2 statistic is inconclusive about the number of Gaussians, is shown for side 1 in Fig. 2b. In general, such behaviour is found for a limited number of cases and, therefore, these results are discarded when determining the number of sediment types. These analyses have been carried out for beam angles between 46° and 60° and for all surveys, not all of which are plotted here. In general, a single outer beam is used to determine the number of Gaussians, but given that our data is noisy, we choose to investigate a number of beams. The use of 7 Gaussians is found to reproduce the measurements best.

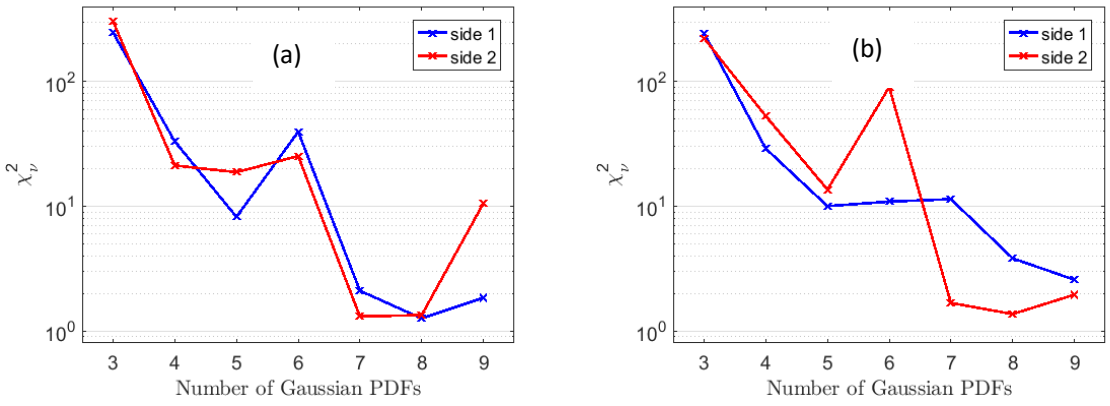

Fig. 2. The reduced χ_ν^2 statistic for the 48° beam angle. The two curves are for the two sides of the echo-sounder respectively. a) 2013 data and b) 2014 and 2015 data.

As an example, Fig. 3 presents the result of the fitting procedure for seven Gaussians. Here the histogram of the measured backscatter data n_j (black line with error bars) per 0.5 dB bin is almost hidden by the modelled backscatter in red. The variance of the measured data is indicated by the error bars. Also seen are the 7 Gaussians used for the curve fitting in black. After a good fit is found per beam angle and per experiment, the intersections of the unscaled Gaussians are used to derive the ranges of backscatter, corresponding to the different acoustic classes, from which the acoustic class map is derived as explained in [23]. Acoustic classes 1-

295 7 correspond to the Gaussians from left to right, and from lowest to highest backscatter
296 values.

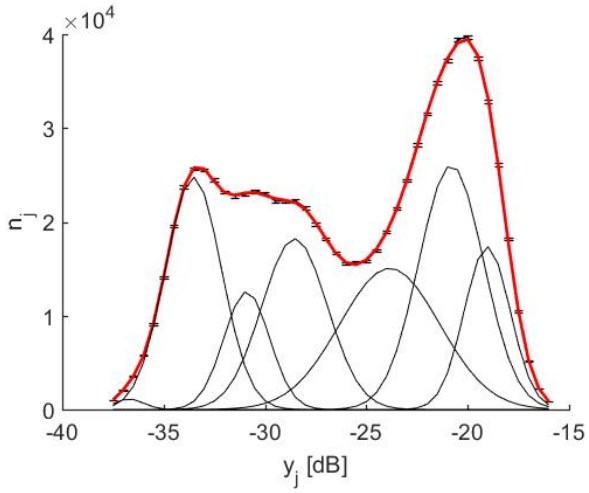

297

298 **Fig. 3. Shown here is the histogram of the measured backscatter data n_j per 0.5 dB bin y_j from the data collected in**
299 **2014 and 2015 (black line with error bars) which is almost hidden by the modelled $f(y_j|x)$ in red. Also displayed are**
300 **the 7 Gaussians in black.**

301

302 The resulting classification map is shown in Fig. 4 where each acoustic class is presented with
303 a separate colour. Colours have been selected such that from green to purple the backscatter
304 value increases.

305 ## 4.2 PCA and k-means clustering

306 PCA in conjunction with a clustering algorithm is a common unsupervised classification
307 technique for seafloor classification based on backscatter [24], [19]. This technique is
308 applicable to relative backscatter values and, therefore, does not necessarily require calibrated
309 MBES. In recent studies, this method was also applied to backscatter and bathymetry
310 simultaneously [20], [4]. However, in this study PCA and k-means clustering are only applied
311 to backscatter so that a direct comparison with the classification from the Bayes method can
312 be made.

313 As with the Bayesian technique, for PCA and k-means clustering, beam angles from 20° to
314 60° are considered. The backscatter data are averaged over seven pings in the along-track
315 direction and over an angle range of 2° to 4° in across-track direction. To eliminate the
316 angular dependency of backscatter the global Z-score approach is applied, which is the
317 subtraction of the mean value from the backscatter value, and then divided by the standard
318 deviation at each angle [20] [42] (henceforth simply referred to as backscatter). To obtain the
319 same resolution among the entire survey area, surface patches of 10 m x 10 m are constructed
320 similar to [32].

321 For each surface patch eight statistical features of the backscatter distribution are calculated
322 (Table 1). The arithmetic mean gives the averaged backscatter value within the patch. If the
323 distribution is not symmetric, the median value differs from the mean and provides the middle
324 of the distribution. Therefore, the median can be considered as an additional valuable feature.
325 The mode represents the value with the highest occurrence within a patch and defines the
326 main tendency of the feature [20]. The standard deviation shows the variability of the
327 backscatter and might be valuable to characterise the heterogeneity of the sediment. Due to
328 the fact that outliers are removed during processing, the minimum and maximum value can be
329 used to define data extremes and might also indicate specific characteristics of the seabed. The
330 higher statistical moments, skewness and kurtosis, are measures of the shape of a probability
331 distribution. In previous studies it was shown that the K-distribution can be used to describe
332 the skewed distribution of backscatter data for all sediment types and the shape parameter of
333 the K-distribution can be used as tool for seafloor classification [43] [44] [32] [45]. Therefore,
334 the skewness and kurtosis might provide valuable information about the sediment distribution.

335 To identify the most valuable of these features, PCA is applied. PCA analysis indicates that
336 the first 3 PCs contain most of the data variability of around 85%. Fig. 5 displays the ratio of
337 the sum of the correlation between the first three PCs and the eight backscatter features to the

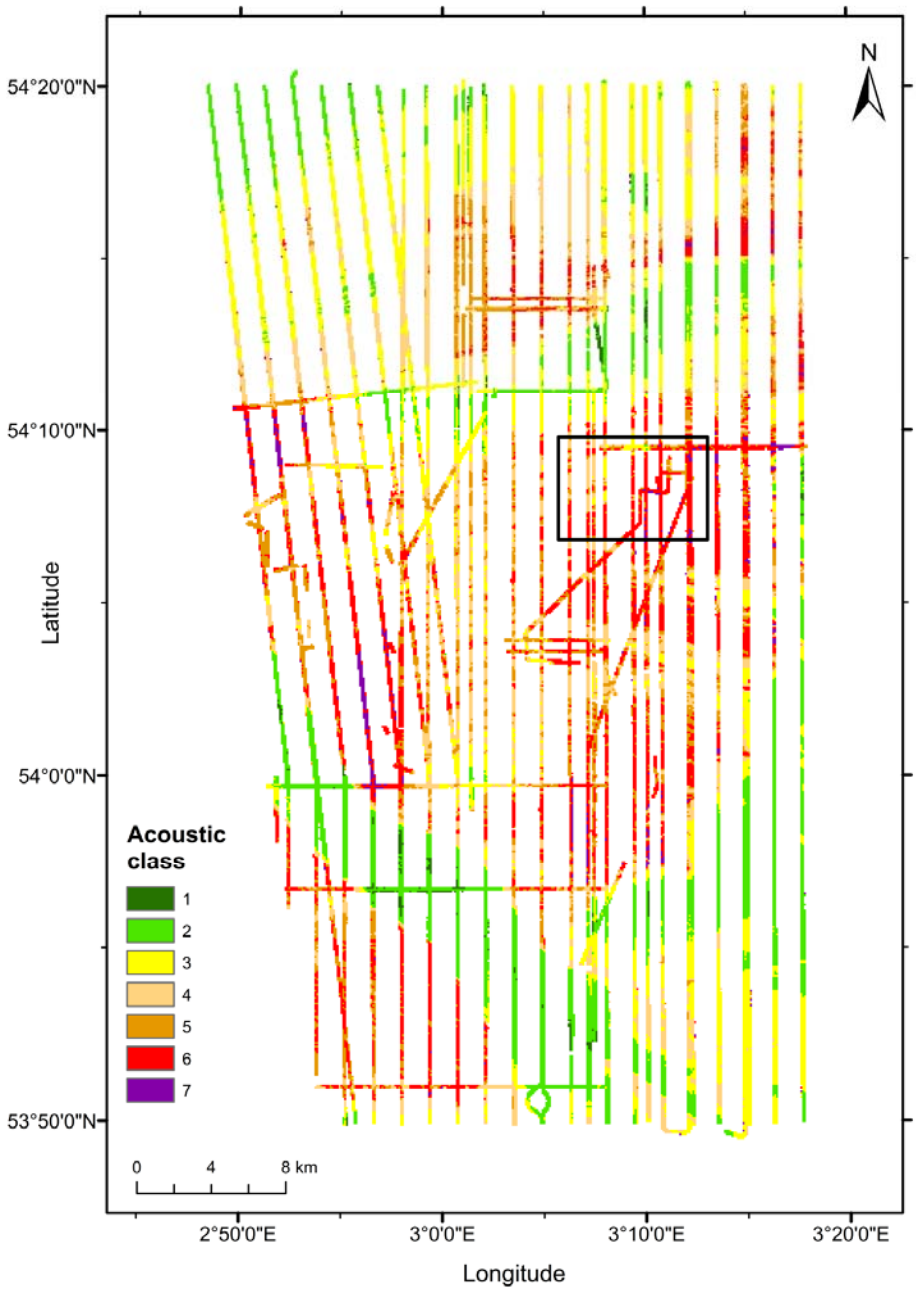

Fig. 4. Acoustic classification result of the Bayesian technique. The grid is resampled to a size of 100 m by 100 m using the mode value of the finer grid. The black square indicates the extent of the area zoomed in Fig. 10.

sum of correlation between the remaining PCs and the eight backscatter features. In reference [20], the threshold value has been chosen considering three conditions: (1) it is similar to the mean value (red line), (2) it includes an adequate number of features for PCA and (3) it

generates consistent results for each survey. Considering these three conditions the mean, median, mode and the minimum of the backscatter data are revealed as the most informative features. PCA analysis indicates that the first 3 PCs contain most of the data variability of around 85%. Fig. 5 displays the ratio of the sum of the correlation between the first three PCs and the eight backscatter features to the sum of correlation between the remaining PCs and the eight backscatter features. In [20], the threshold value has been chosen considering three conditions: (1) it is similar to the mean value (red line), (2) it includes an adequate number of features for PCA and (3) it generates consistent results for each survey. Considering these three conditions the mean, median, mode and the minimum of the backscatter data are revealed as the most informative features.

Table 1. Backscatter features considered in the first application of PCA.

Number	1	2	3	4	5	6	7	8
BS feature	Mean	Std. deviation	Skewness	Kurtosis	Median	Mode	Min.	Max.

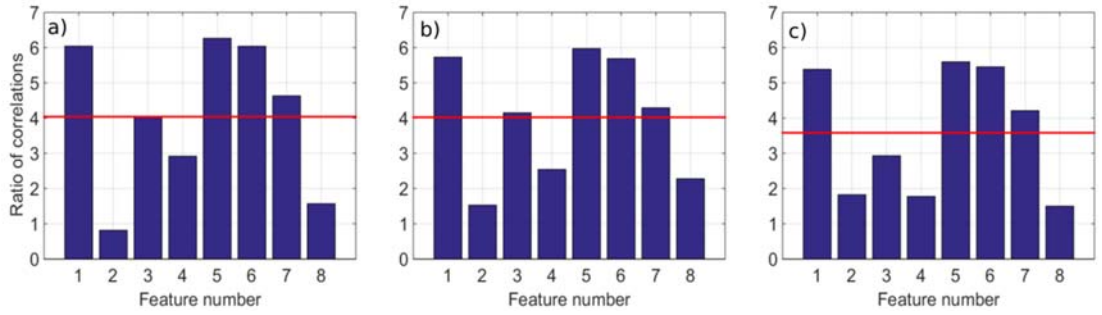

Fig. 5. Ratio of the sum of the correlation between the first 3 PCs and backscatter features to the sum of the correlation between the remaining PCs and backscatter features. The different surveys are considered separately: a) 2013, b) 2014 and c) 2015. The red line indicates the mean value of the ratio of correlation.

These features were used as an input for a second application of PCA to further reduce the complexity of the dataset and simplify the application of the k-means clustering. The analysis shows that the first PC accounts for 98% of the data variability which indicates high correlation between the selected four backscatter features. Therefore, only this component is used in the k-means clustering.

364 To estimate the optimal number of acoustic classes that can be distinguished within the data,
365 the gap statistic, silhouette coefficient and Davies-Bouldin method are applied. The methods
366 use the output of the k-means algorithm which is applied to varying numbers of clusters in the
367 range from 2 to 10. The results of each method are plotted in Fig. 6. Each method has
368 different magnitudes of criterion values and therefore the values are normalised. The optimal
369 number of classes estimated and suggested by each method is two, which is indicated by the
370 red dots. This can be understood from Fig. 3, showing a histogram of the backscatter data.
371 Clearly two main peaks are present. These two main peaks are estimated as individual clusters
372 by the statistical methods. However, this is in disagreement with both the ground truth data
373 which reveals eight sediment types, and the Bayesian technique which estimates seven
374 clusters, similar to the ground truth data.

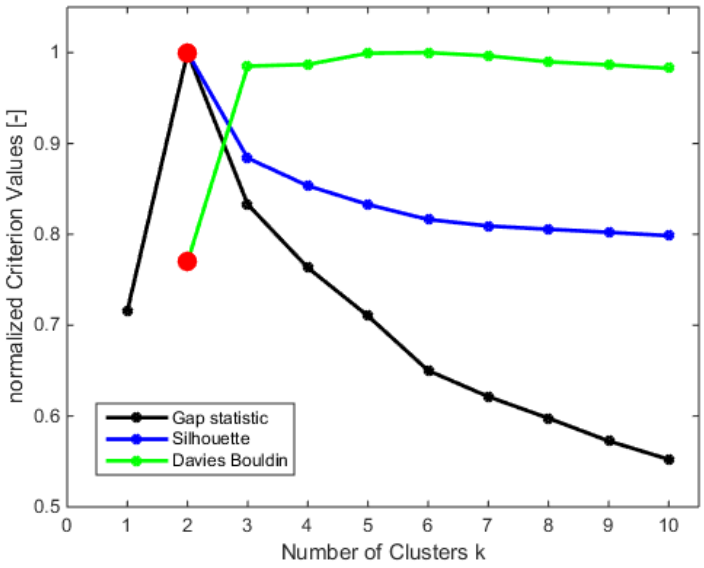

375

376 **Fig. 6. Estimating the number of clusters via Gap statistics, Silhouette coefficient and Davies-Bouldin method. Red**
377 **circle indicates optimal number of clusters estimated by each method.**

378 To further investigate why the statistical methods only identify two clusters within the
379 backscatter data the Gap statistics, Silhouette coefficient and Davies-Bouldin methods are
380 applied to synthetic backscatter histograms. Four different synthetic backscatter histograms
381 with varying degree of overlap and number of main peaks are shown in Fig. 7. Fig. 7c

represents a similar backscatter histogram as the measured histogram (Fig. 3). Again, the methods only identify the two main peaks as individual clusters. Modelling backscatter histograms with four and seven main peaks, respectively (Fig. 7b and Fig. 7d) and applying the statistical methods show that even when the individual peaks are clearly visible, the overlap hampers the clustering methods' ability to identify the peaks as individual clusters. Only the synthetic backscatter histogram in Fig. 7a having peaks with very distinct separations were correctly found to have four clusters by the three methods. This demonstrates that the statistical methods trying to estimate the number of clusters require a clear segmentation of the individual clusters which is not always the case for backscatter data. Seafloor backscattering is a random process having statistical fluctuation leading to a natural overlap of the backscatter data [1]. In addition, the mostly heterogeneous seabed does not show clear boundaries between sediment types, increasing the overlap within the measured backscatter data. In this study, the backscatter features are highly correlated. It is hypothesized that for situations where this correlation is less, or when additional information such as those derived from bathymetry are added, the overlap in clusters diminishes and separation between clusters would be higher. The Bayesian technique accounts for the statistical fluctuation of the backscatter data [23] and, therefore, is able to distinguish between individual overlapping clusters in this study as well. This method estimates seven clusters to be present in the data set. Based on the result of the Bayesian technique and taking into account the fact that the ground truth data reveals eight sediment types (defined by the Folk scheme) (Section 4.3) as well as to have consistency between the Bayes and PCA/k-means methods, k-means clustering is applied with a choice of seven clusters.

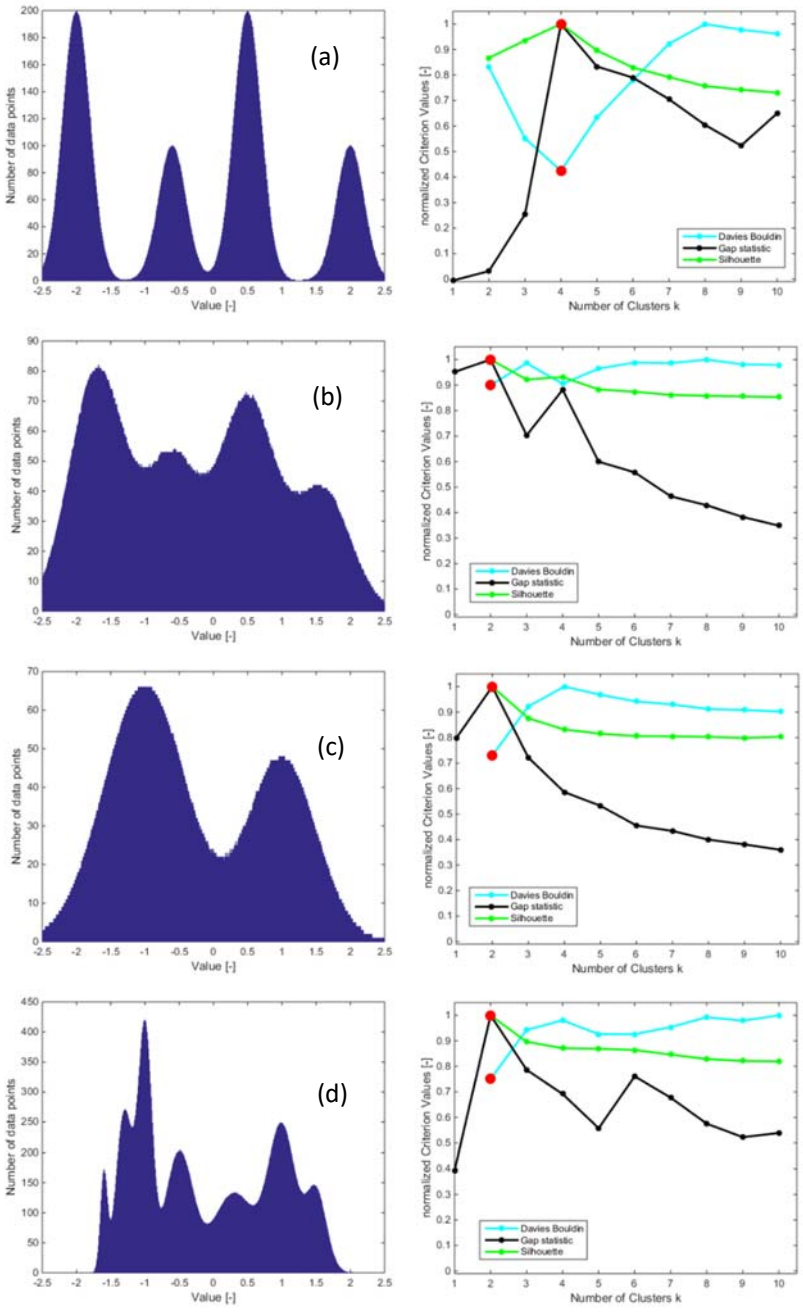

404

405 **Fig. 7 Synthetic histograms generated by modelling a different number of Gaussians (left). Application of Davies**
406 **Bouldin, Gap statistic and Silhouette coefficient to synthetic data (right). (a) 4 clearly segmented Gaussians. Each**
407 **statistical method gives 4 clusters as a result. (b) 4 Gaussians with overlapping segmentation. Statistical methods are**
408 **not able to identify 4 individual clusters. (c) 2 Gaussians representing a hypothetical histogram of backscatter data of**
409 **the Cleaver Bank. Statistical methods identify 2 clusters. (d) 7 Gaussians that approximately reproduce the histogram**
410 **of the backscatter data of the Cleaver Bank but with added separation. Even in this modelled and simplified case,**
411 **statistical methods suggest 2 clusters as the optimal number.**

412 Acoustic classes are obtained from the output of the k-mean clustering by sorting the seven

413 clusters according to the averaged backscatter value of each cluster. Fig. 8 displays the

414 resulting acoustic classification map. Compared to the acoustic map of the Bayesian approach
415 (Fig. 4) acoustic class 1 and 7 have a very large contribution to the entire map. The resulting
416 map can be divided in seven distinct areas based on the criterion of high and low acoustic
417 classes as well as homogeneity and heterogeneity. The most of obvious areas are 1) the
418 heterogeneous centrum consisting of mainly acoustic classes with higher backscatter values;
419 2) and 3) the homogenous north-western and south-eastern parts with lower backscatter
420 values; 4) the very homogeneous Botney cut characterised by only acoustic class number 1 in
421 the south of the central part; 5) the south-western area which is characterised by
422 homogeneously distributed sediments with high backscatter values; and 6) just north of the
423 centre a stripe of low backscatter, homogeneously distributed sediment is located; 7) further
424 north in the north-eastern part of the map a very small stripe of heterogeneous, high acoustic
425 classes, sediment is present. These distinct areas are also visible in the acoustic map of the
426 Bayesian technique (Fig. 4). The main differences to consider belong to a shift between the
427 acoustic classes, in particular at the low and high classes. A more detailed view and
428 discussion of these maps follows in sections 5.1 and 5.3.

429 **4.3 Ground truth**

430 The analyses of the grab samples indicate the presence of eight different sediment Folk
431 classes, ranging from sandy mud to sandy gravel in the Cleaver Bank. The grab samples
432 containing gravel are located in the northern and middle part of the survey area as well as in
433 the south of the Botney cut (see Fig. 13). Sandy mud grab samples are only available within in
434 the Botney cut and muddy sand occurs mainly around the Botney cut. The grab samples from
435 2013 to 2015 are located directly on the MBES track whereas some grab samples taken in
436 2000 are located about 500 m away from a MBES survey line (Fig. 1).

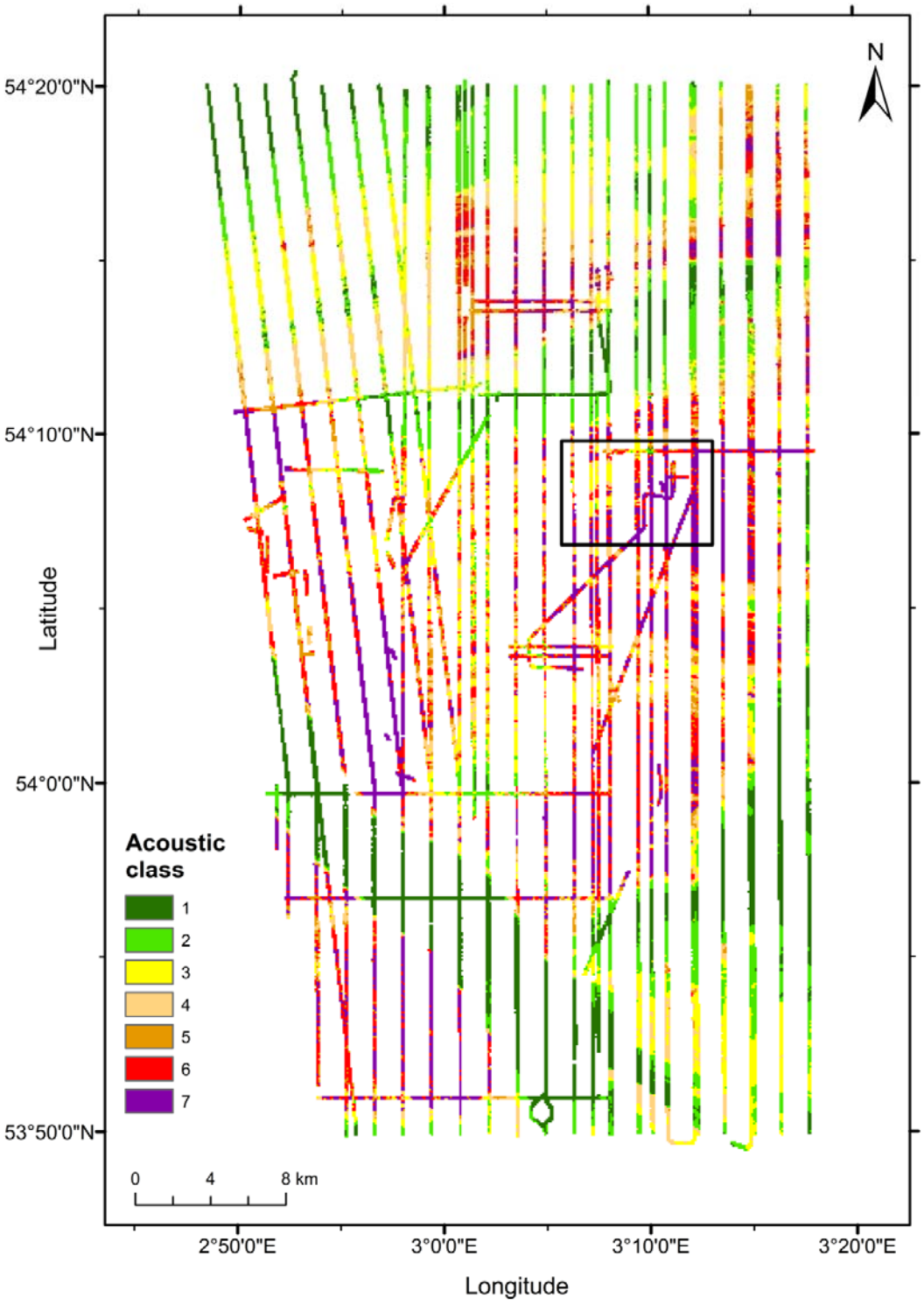

437

438 **Fig. 8. Acoustic classification result of PCA in conjunction with k-mean clustering using 7 acoustic classes. The grid is**
439 **resampled to a size of 100 m by 100 m. The black square indicates the extent of the area zoomed in Fig. 9 and Fig. 10.**

5. Discussion

In this section the repeatability of the classification results is discussed by comparing the different surveys. The assignment of acoustic classes to sediment classes based on the correlation of ground truth data with acoustic classes is also examined. Furthermore, the spatial resolution and the reliability of the classification results is analysed. Finally, the relationship between median grain size and backscatter values is investigated.

5.1 Repeatability and consistency of classification results

In order to examine the repeatability of the classification results over the different surveys, a small area of the Cleaver Bank is shown in Fig. 9 and Fig. 10 with a total of ten intersections of survey lines. All five surveys are represented in this small area of the map. Clearly there is a high agreement in the classification results obtained from the data from different surveys. Examples are the intersection of the easternmost 2013 week 45 vertical line that intersects with the 2015 diagonal line (indicated by area D in the plot). In this intersection features as narrow as eight meters are clearly visible and are in very good agreement for the two surveys. At the intersection of the most western 2013 week 45 line and the 2013 week 47 line (area A) both surveys show an area of acoustic class 3, surrounded by class 6. Area B indicates for both surveys the presence of acoustic classes 2 to 6 in good agreement. The high repeatability is also apparent in Fig. 11. Here the Bayes acoustic classes determined for the intersecting areas of the 2013 and 2014/2015 surveys are presented in a scatter plot. It is shown that for the majority of the cases the results are in good agreement. However, discrepancies also occur, for example at the intersection of the 2015 survey and the 2013 week 47 survey in area C of Fig. 9 and 10 the 2013 data shows acoustic class 2 whereas the 2015 data shows acoustic class 1 for PCA. The Bayesian results in this intersection show class 3 for the 2013 data and class 2 for the 2015 data. This is the most apparent disagreement seen on this part of the map,

464 and there are a few plausible explanations for this and other disagreements. Firstly, even
465 though it would not be expected, it is possible that there was a sediment change from 2013 to
466 2015, that would explain why the discrepancy is present for both classification methods in
467 area C. To prove a sediment change at any point a grab sample from both periods at the
468 location would be required but this is not available. According to Fig. 11 there are
469 discrepancies between the 2013 and the 2014/2015 data but they are not greater than 1
470 acoustic class except for 1 instance. It is possible that the backscatter from locations with
471 different classifications are close to a class boundary and happen to fall within the 1 class
472 discrepancy range. A further reason for a mismatch could be a directional small-scale
473 morphological influence because of different sailing directions [46]. Given that this is data
474 from five different surveys carried out over the time period from 2013 to 2015 and that the
475 data were acquired by different vessels, crews, MBES systems and environmental conditions,

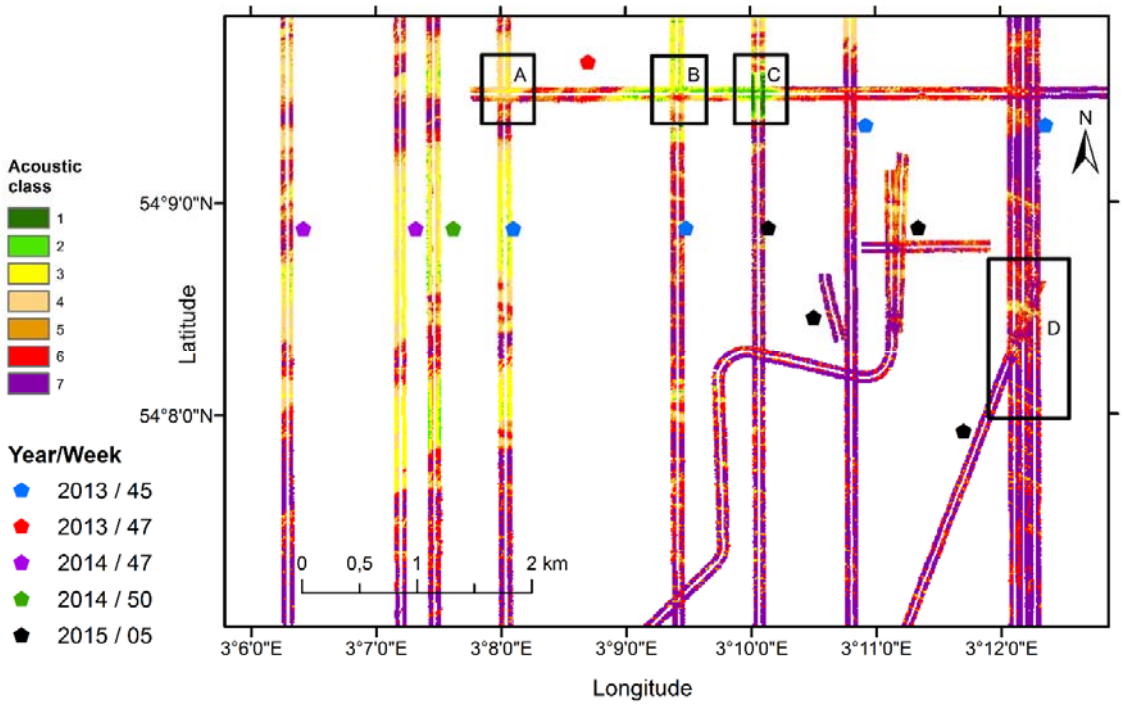

476

477 **Fig. 9. Zoomed in area of acoustic class map generated by PCA. Different survey lines denoted by the coloured**
478 **pentagons are visible. The grid size is 10 by 10 m and represents the size of the surface patches.**

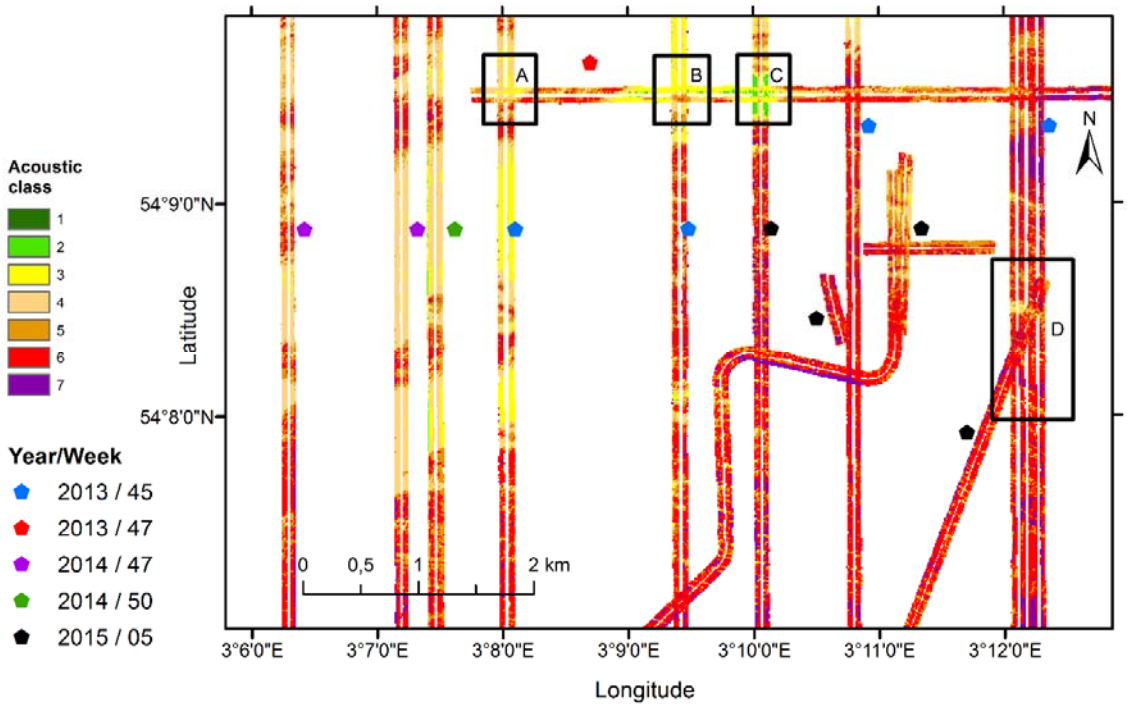

Fig. 10. Zoomed in area of acoustic class map generated by Bayesian technique. Different survey lines denoted by the coloured pentagons are visible. The grid is resampled to a size of 10 m by 10 m using the mode value of the finer grid.

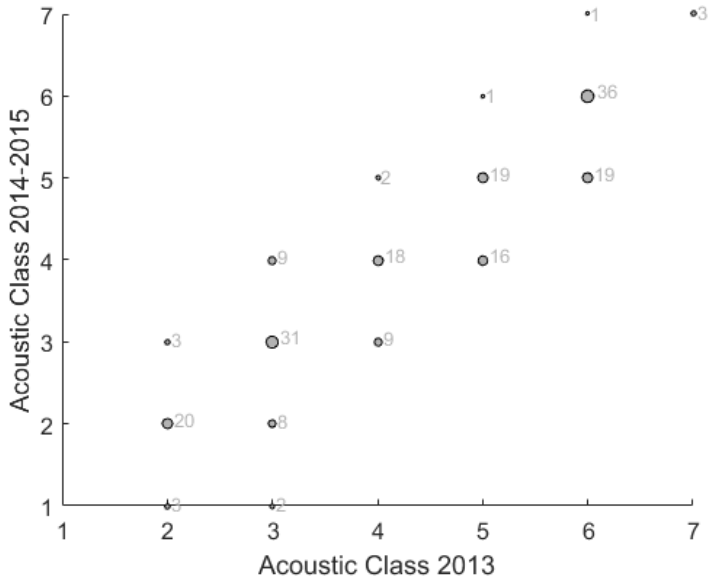

Fig. 11. Correlation plot of the acoustic classes determined with the Bayesian method. The size of the dots and the number indicate the number of matches for the acoustic classes determined for the intersecting areas using the backscatter data from the different surveys in 2013, 2014, 2015.

the results still demonstrate the high degree of repeatability and consistency of the acoustic classifications for both methods. Although the classification results are in good agreement

when comparing the classification from different surveys for one method, the comparison between classification results from applying different methods reveals differences. Whereas the Bayes classification indicates the presence of mainly five types of sediments, since acoustic classes 1 and 7 are hardly present, the PCA classification shows all sediment types to be almost equally present. The deviations from PCA and Bayesian within the low and high acoustic class ranges are related to the different mathematical approaches of the methods. Considering Fig. 3, it is seen that the PDFs of acoustic class 1 and 7 have only a very small contribution to the histogram of backscatter measurements. For k-means clustering 7 sediment types are assumed. K-means clustering defines the clusters on a simple similarity measurement of the first PC and assigns these clusters based on an increasing backscatter value. This leads to a more balanced number of data points within the individual clusters, i.e., acoustic classes. Therefore, the PCA results show, in contrast to Bayes, a significant presence of acoustic class 1 and 7. Still, the maps obtained with the two different methods indicate a similar spatial distribution of the different sediment types over the area.

5.2 Mapping Folk class by combining acoustic classes with ground truth data

Often, for mapping the spatial distribution of sediments, use is made of maps presenting the Folk class. Here it is investigated to what extent these types of maps can be derived from the acoustic classification results by assigning sediment types to the acoustic classes. For this, we use the grab samples that are located at a distance less than 25 m from a survey track, i.e. slightly more than the 20 m recommended in [46], and that are in areas with little spatial variation in sediment type. As such, the initial 104 grab samples (Fig. 1) are reduced to 77 grab samples.

As a first step, it is assumed that the lowest acoustic class represents finer sediments whereas the highest acoustic class represents coarser sediments. Here the order of Folk classes is

selected such that it is assumed to represent increasing median grain size. The resulting number of matches between acoustic class number and sediment type at the grab sample location are plotted in Fig. 12 for the Bayes and PCA results, respectively. In general, indeed increasing acoustic class is seen to correspond to an increasing median grain size, as represented by the sediment type.

The PCA results show a good match of acoustic class 1 with the sediment type sandy mud. For example, this indicates that the Botney cut is covered by sandy mud. However, the assignment of the sand sediment types from muddy sand to sandy gravel are less clear. For instance, the sediment type sand shows a uniform distribution from acoustic class 1 to 5. This indicates additional factors influencing the backscatter data and causes difficulties in the assignment of sediment type sand to a distinct acoustic class. For the Bayes results (Fig. 12a) it is found that acoustic class 1 does not correlate to any grab sample. For all other acoustic classes there is some ambiguity in the relation between sediment type and acoustic class.

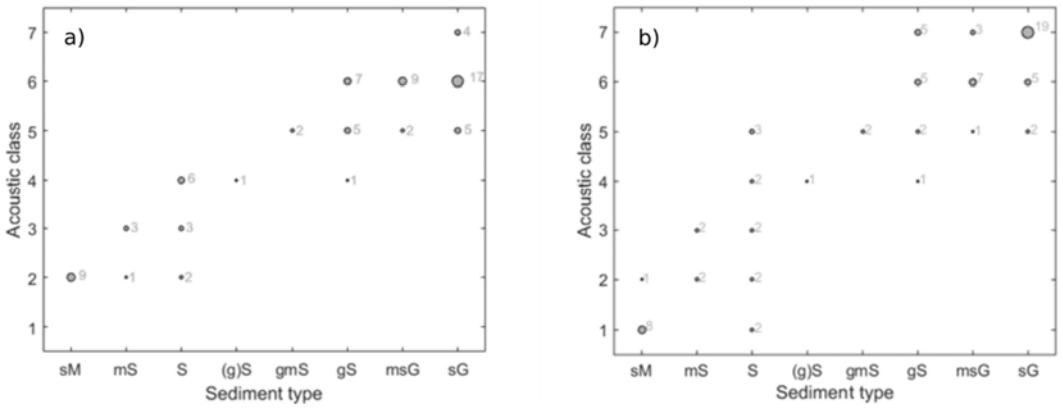

Fig. 12. Correlation between acoustic class and sediment type at grab sample locations. a) Bayesian method, b) PCA. Dots indicate the number of matches between acoustic class and sediment type. The sediment type is determined after Folk [22].

Fig. 13 shows the Folk class map based on the Bayes classification accounting for the mentioned non-uniqueness. The proposed assignment of Folk class to sediment type used is presented in table 2. It should be noted, however, that especially for acoustic class 5 a unique relation with Folk class is not found and for Fig. 13 it is taken to correspond mainly to

533 gravelly sand and muddy sandy gravel. A similar map can be made for the results of PCA, but
534 here only the Bayes results in Fig. 13 are presented.

535 **Table 2 Assignment of sediment type (Folk scheme) to acoustic class. Acoustic classes are obtained from applying the**
536 **Bayes classification method.**

Sediment type	**sM** sandy mud	**mS** muddy sand	**S** sand	**gmS** gravelly muddy sand	**gS** gravelly sand	**msG** muddy sandy gravel	**sG** sandy gravel
Acoustic class	2	3	4	5	5-6	5-6	6-7

537

538 ## 5.3 Spatial resolution of classification results

539 To investigate the scale of information obtained from the acoustic classification, Fig. 13
540 shows more detailed pictures of selected areas in the Cleaver Bank. These areas are selected
541 because grab samples are available and abrupt changes in the acoustic class occur within a
542 mainly homogeneous area. Whereas, on the main sediment map the high resolution and the
543 agreement between grabs sample and classification result are not obvious, the zoomed in plots
544 do demonstrate these items. Each picture depicts strong changes in sediment classes over tens
545 of meters resolved by the acoustic classification method. The sediment type of the grab
546 samples denoted by the coloured squares matches well with the classification result. In
547 particular, Fig. 13b shows an abrupt change in the sediment map which matches perfectly
548 with the ground truth given sandy gravel and sand as a sediment type. It is notable that the
549 sand grab sample is only approximately 10 m away from the estimated sand to gravel
550 boundary but is perfectly resolved on the sediment map. Fig. 13c displays an area which
551 seems to be a homogeneous sandy mud to muddy sand region on the main map but the
552 detailed view reveals a gravelly sediment patch within this area. This patch matches very well
553 with the grab sample of muddy sandy gravel. The detailed pictures display only a few
554 examples of the match between classification result and grab sample. The main map of the
555 Cleaver Bank, in general, also shows good agreement between classification results and

556 ground truth. For instance, the Botney cut is classified with sandy mud which fits to each grab
557 sample taken in that area.

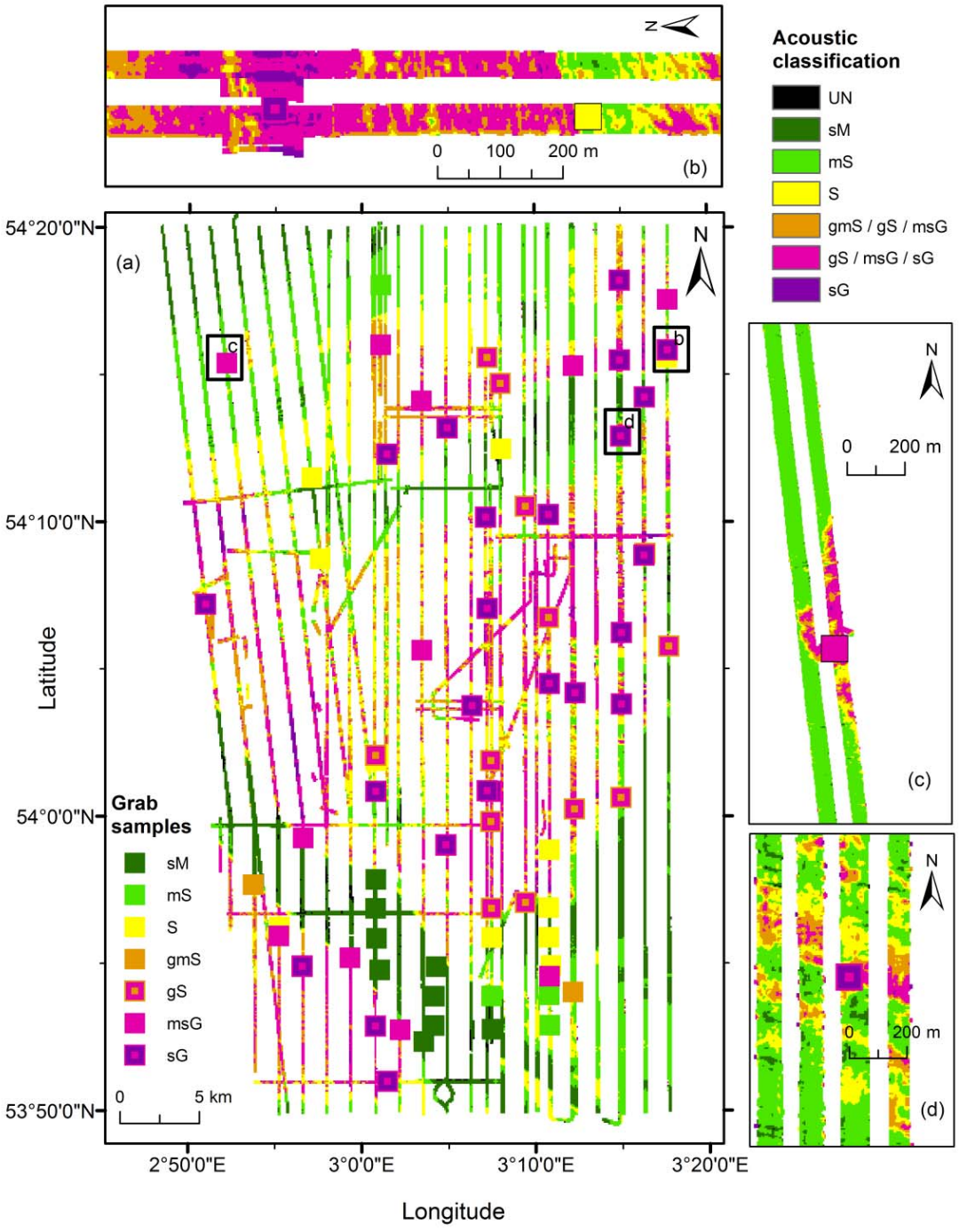

558

559 **Fig. 13. Sediment map of the Cleaver Bank obtained from the Bayesian method and ground truth data. Sediment**
560 **classes range from sandy mud (sM) to sandy gravel (sG). a) Sediment map of the entire survey area of the Cleaver**
561 **Bank with a resolution of 100 m by 100 m. b), c) and d) represent small areas of the sediment map with a resolution of**
562 **3 m by 3 m. The grab samples can be seen in the main map as a colour coded squares.**

563 ### 5.4 Relation of acoustic classes with sediment median grain size

564 In Section 5.2 the relation between acoustic class and Folk class is investigated. It is found
565 that no unique relation holds for the frequency and sediments considered in this study.
566 Therefore, in this section it is investigated whether a more unique relationship between
567 acoustic class and median grain size exists. To this end, the median grain sizes (D50 value) of
568 the grab samples are now considered as in [47]. Except for class 7, the median values increase
569 with class number as seen in Fig. 14 which presents the median of the D50 values as a
570 function of acoustic class. This reflects an increasing backscatter value with increasing class
571 number. Class 7 does not have a mean or median value higher than that of class 6. This
572 indicates a situation where the highest backscatter values (class 7) apparently correspond to
573 median grain sizes that are not necessarily higher than those belonging to class 6. Based on
574 this result it can be concluded that, especially for the higher acoustic classes, as for the Folk
575 class also no unique relationship between acoustic class and median grain size exists in the
576 data.

577 To further investigate this we consider standardized backscatter values instead of acoustic
578 class. In Fig. 15 the backscatter values (averaged over measurements within 25 m around a
579 grab sample location) are shown as a function of D50 values. The backscatter values are
580 additionally normalized by dividing each backscatter value by the maximum backscatter value
581 thus yielding values strictly between -1 and 1. Fig. 15 shows a significant positive correlation
582 between backscatter and median grain size for the fine fraction (< 1ϕ (0.5 mm)). From the
583 data, however, it is found that the magnitude of increase in backscatter with increasing median
584 grain size is less significant between 1 and -1 ϕ (0.5 mm - 2 mm), followed by a plateau and a
585 decrease for even coarser sediments. This indicates an ambiguity for the relationship between
586 backscatter values and median grain size exists and hinders the discrimination of sediment
587 types with median grain sizes larger than 1 ϕ (0.5 mm) using acoustic classification methods

588 based only on backscatter data. This is in agreement with the findings of section 5.2. and
589 indicates that there is no one-to-one relationship between median grain size and backscatter
590 for the entire grain size spectrum. Such a positive correlation between backscatter and median
591 grain size followed by a negative correlation was also observed in [4]. They referred to this
592 change in relationship as a transition point. The transition point in the study of [4] occurred at
593 -3.5 ϕ (11 mm) using a frequency of 300 kHz. We estimate the transition point at
594 approximately -2 ϕ (4 mm). The transition point in [4] and the transition point in this study
595 both occur roughly around the acoustic wavelength (5 mm) of the MBES.

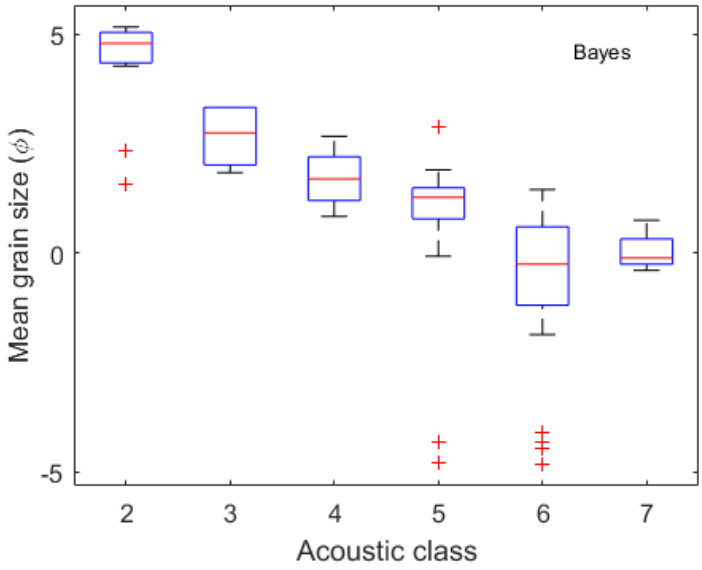

596

597 **Fig. 14. Box plots of sediment samples that fall within the same acoustic class. The bottom and top of the blue**
598 **rectangle represent the 25th and 75th percentiles, respectively, whereas the red line indicates the median value. The**
599 **whiskers extend to the minimum and maximum value of the D50 values that are not considered outliers (i.e. they are**
600 **no more than ±2.7σ apart). Outliers are marked with red crosses. The results for PCA, not plotted, are very similar.**

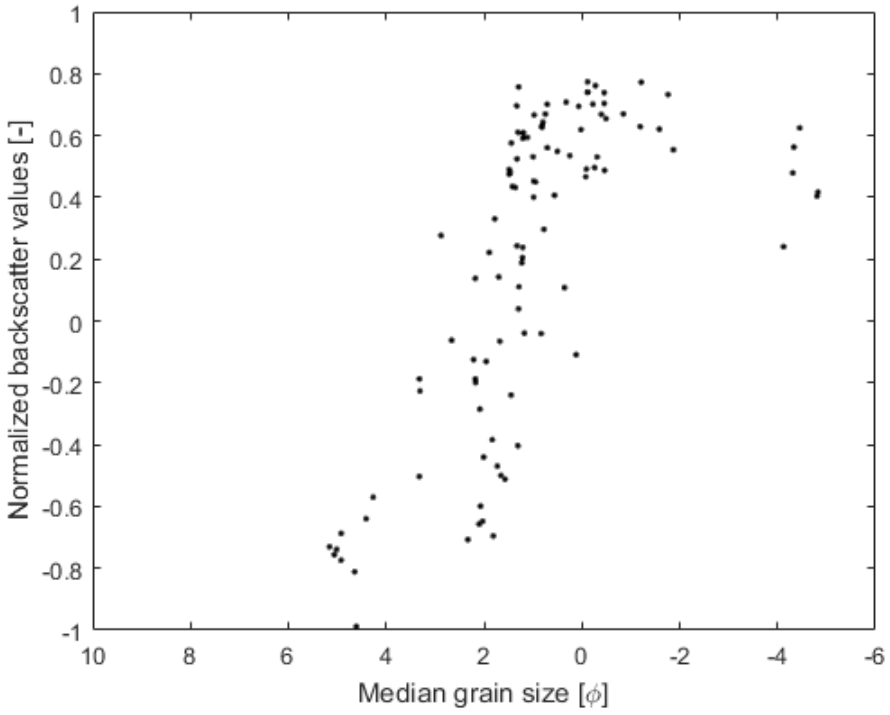

601

602

603 **Fig. 15. Backscatter values as a function of the median grain size (D50) of grab samples. Dots indicate the averaged**
604 **and standardized backscatter values within a maximum radius of 25 m around the grab sample.**

605

606 ## 6. Summary and conclusions

607 In this study two different acoustic classification methods, namely the Bayesian method and
608 the PCA in conjunction with k-means clustering, were applied to MBES backscatter data from
609 the Cleaver Bank in the Dutch North Sea. For both methods, the classification is based on
610 changes in backscatter values for different sediment types. The data were acquired on two
611 different Dutch vessels during five different surveys carried out in various time periods from
612 2013 to 2015.

613 The resulting maps show a high consistency between the classification results obtained from
614 the different surveys and using a single classification method, despite the use of different
615 vessels and varying time periods. Some discrepancies are observed (a difference of 1 acoustic

616 class); to gain a better understanding of these would require repeated surveys following the
617 same survey patterns and supported by repeated grab samples for each of those surveys.
618 Despite the discrepancies, this study demonstrates the potential of using backscatter data for
619 achieving repeatable seabed sediment classification results even if the backscatter data is
620 acquired during different time periods and from MBES systems which are mounted on
621 different ships and thus subjected to different calibrations, survey settings, and ship crews. It
622 can be concluded that the current state of MBES sediment classification techniques is such
623 that it can be applied for marine sediment monitoring purposes where the aim is to identify
624 changes in the sediment over time.

625 However, the current study clearly shows that monitoring requires the use of a single
626 classification technique. Although, the same large-scale features are resolved, the two
627 different techniques result in different maps. For the two techniques considered and using
628 backscatter data only, the difference fully stems from the different approaches used for
629 assigning backscatter measurements to a certain acoustic class. The Bayesian technique
630 accounts for the statistical characteristics of the backscatter by assuming Gaussian distributed
631 backscatter values. Whereas PCA in conjunction with the k-means algorithm uses a cluster
632 technique to classify a dataset with respect to similarities of predefined properties and,
633 thereby, neglects the natural fluctuation of backscatter which can superimpose the backscatter
634 variation due to different seabed properties. The latter was found to underestimate the number
635 of sediment types within the study area. Still, if additional information, such as bathymetry
636 derived features, is considered the PCA method becomes an essential tool due to the ability of
637 selecting the most valuable features [4], [20].

638 Finally, it was investigated to what extent Folk classes and median grain sizes can be assigned
639 to acoustic classes. In general, this step is hindered by the fact that sediment bulk density,
640 seafloor roughness, volume heterogeneity, discrete scatterers and sediment layering all

contribute to backscatter strength depending on the seabed complexity, acoustic frequency and incident angle [1], [2], [3]. For the Cleaver Bank area and the multi-beam (300 kHz) considered here, no unique relation between Folk class and acoustic class could be established. To still be able to map Folk class, a conversion scheme accounting for this non-uniqueness was introduced where a range of Folk classes is assigned to a single acoustic class. With regards to the relationship between median grain size and backscatter (acoustic class), a strong positive correlation for the fine fraction (< 0.5 mm) followed by a decrease in positive correlation and a change into negative correlation for coarser sediments (> 4 mm) are observed. This constitutes an ambiguity in the relationship between backscatter and median grain size. Therefore, care must be taken when assigning sediment properties or types (e.g. median grain size or Folk class) to an acoustic class based on MBES backscatter.

In conclusion, although limitations exist, current seafloor classification capabilities are such that they are a valuable asset in long-term monitoring efforts of the marine environment.

7. Acknowledgements

The authors would like to thank the crews of the Zirfaea and the Arca of Rijkswaterstaat for their role in acquiring the data in the Cleaver Bank. Ad Stolk of Rijkswaterstaat is especially acknowledged for his part in both organizing the data gathering campaigns as well as making the data available for research.

661 **Bibliography**
662

[1] D. R. Jackson and M. D. Richardson, High-Frequency Seafloor Acoustics, New York: Springer Science, 2007.

[2] A. N. Ivakin, “Scattering from discrete inclusions in marine sediments,” in *Proc. Seventh European Conference on Underwater Acoustics. Delft University of Technology*, Delft, The Netherlands, 2004.

[3] K. L. Williams, D. R. Jackson, D. Tang, K. B. Briggs and E. I. Thorsos, “Acoustic backscattering from a sand and a sand/mud environment: Experiments and data/model comparison,” *IEEE Journal of Oceanic engineering,* vol. 34, no. 4, pp. 388-398, 2009.

[4] D. Eleftherakis, M. Snellen, A. Amiri-Simkoeei and D. G. Simons, “Observations regarding coarse sediment classification based on multi-beam echo-sounder's backscatter strength and depth residuals in Dutch rivers,” *J. Acoustic. Soc. Am.,* vol. 135, no. 6, pp. 3305-3315, 2014.

[5] J. S. Collier and C. J. Brown, “Correlation of sidescan backscatter with grain size distribution of surficial seabed sediments,” *Marine Geology,* vol. 214, no. 4, pp. 431-449, 2005.

[6] G. De Falco, R. Tonielli, G. Di Martino, S. Innangi, S. Simeone and I. M. Parnum, “Relationships between multibeam backscatter, sediment grain size and Posidonia oceanica seagrass distribution,” *Continental Shelf Research,* vol. 30, pp. 1941-1950, 2010.

[7] J. A. Goff, H. C. Olson and C. S. Duncan, “Correlation of side scan backscatter intensity with grain size distribution of shelf sediments,” *Geo-marine Letters,* vol. 20, pp. 43-49, 2000.

[8] T. Medialdea, l. Somoza, R. F. M. Leon, G. Ercilla, A. Maestro, D. Casas, E. Llave, F. J. F.-P. M. C. Hernandez-Molina and B. Alonso, “Multibeam backscatter as a tool for sea-floor characerization and identification of oil spills in the Galicia Bank,” *Marine Geology,* vol. 249, pp. 93-107, 2008.

[9] D. G. Simons, M. Snellen and M. Ainslie, “A multivariate correlation analysis of high-frequency bottom backscattering strength measurements with geotechnical parameters,” *IEEE J. Ocean. Eng.,* vol. 32, pp. 640-650, 2007.

[10] B. D. Edwards, P. Dartnell and H. Chezar, “Characterizing benthic substrates of Santa Monica Bay with seafloor photography and multibeam sonar imagery,” *Marine Environmental Research,* vol. 56, no. 1-2, pp. 47-66, 2003.

[11] V. E. Kostylev, R. C. Courtney, G. Robert and B. J. Todd, “Stock evaluation of giant scallop (Placopeceton magellanicus) using high-resolution acoustics for seabed mapping,” *Fisheries Research,* vol. 60, no. 2-3, pp. 479-492, 2003.

[12] J. C. Borgeld, J. E. Hughes Clark, J. A. Goff, L. A. Mayer and J. A. Curtis, “Acoustic backscatter of he 1995 flood deposit on the Eel shelf,” *Marine Geology,* vol. 154, pp. 197-210, 1999.

[13] F. O. Nitsche, R. Bell, S. M. Carbotte, W. B. F. Ryan and R. Flood, “Process-related classification of acoustic data from the Hudson River Estuary,” *Marine Geology,* vol. 209, pp. 131-145, 2004.

[14] L. Fonseca, L. Mayer, D. Orange and N. Driscoll, “The high-frequency backscattering angular response of gassy sediments: model/data comparison from Eel River Margin, California,” *The Journal of the Acoustical Society of America,* vol. 111, no. 6, pp. 2621-2631, 2002.

[15] K. Siemes, M. Snellen, A. R. Amiri-Simkooei, D. G. Simons and J.-P. Hermand, “Predicting Spatial Variability of Sediment Properties From Hydrographic Data for Geoacoustic Inversion,” *IEEE Journal of Oceanic Engineering,* vol. 35, no. 4, pp. 766-778, 2010.

[16] C. McGonigle and J. Collier, “Interlinking backscatter, grain size and benthic community structure,” *Estuar. Coast. Shelf Sci.,* vol. 147, pp. 123-136, 2014.

[17] D. D. Sternlicht and C. P. de Moustier, “Remote sensing of sediment charactristics by opitmized echo-envelope matching,” *The Journal of the Acoustical Society of America,* vol. 114, no. 5, pp. 2727-2743, 2003.

[18] L. Fonseca, C. Brown, B. Calder, L. Mayer and Y. Rzhanov, “Angular range analysis of acoustic themes from Stanton banks Ireland: a link between visual interpretation and multibeam echosounder angular signatures,” *Applied Accoustic,* vol. 70, pp. 1298-1304, 2009.

[19] C. J. Brown, B. J. Todd, V. E. Kostylev and R. A. Pickrill, “Image-based classification of multibeam sonar backscatter data for objective surficial sediment mapping of Georges Bank, Canada,” *Continental Shelf Research,* vol. 31, pp. 110-119, 2010.

[20] D. Eleftherakis, A. Amiri-Simkooei, M. Snellen and D. G. Simons, “Improving riverbed sediment classification using backscatter and depth residual features of mulit-beam echo-sounder systems,” *J. Acoust. Soc.,* vol. 131, no. 5, pp. 3710-3725, 2012.

[21] J. Anderson, D. van Holliday, R. Kloser, D. Reid and Y. Simard, “Acoustic seabed classification: current practice and future directions,” *ICES Journal of Marine Science,* vol. 65, pp. 1004-1011, 2008.

[22] C. J. Brown, S. J. Smith, P. Lawton and J. T. Anderson, “Benthic habitat mapping: A review of progress towards improved understanding of the spatial ecology of the seafloor using acoustic techniques,” *Estuarine, Coastel and Shelf Science,* vol. 92, pp. 502-520, 2011.

[23] D. G. Simons and M. Snellen, “A Bayseian approach to seafloor classification using multi-beam echo-sounder backscatter data,” *Applied Acoustics,* vol. 70, pp. 1258-1268, 2009.

[24] E. Alevizos, M. Snellen, D. G. Simons, K. Siemens and J. Greinert, “Acoustic discrimination of relatively homogeneous fine sediments using Bayesian classification on MBES data,” *Marine Geology,* vol. 370, pp. 31-42, 2015.

[25] E. Heffron, M. Doucet, C. Brown, G. Lamarche and R. Cooper, “Multibeam Backscatter Workshop - State of the Technology, Tools & Techniques: Overview,” GeoHab Annual Conference,

Fiorentino, A., Rome, Italy, 2013.

[26] X. Lurton, G. Lamarche, C. Brown, V. Lucieer, G. Rice, A. Schimel and T. Weber, “Backscatter measurements by seafloor-mapping sonars. Guidelines and Recommendations,” 2015.

[27] H. J. Lindeboom, R. Witbaard, O. G. Bos and E. Meesters, “Gebiedsbescherming Noordzee. Habitattypen, instandhoudingsdoelen en beheersmaatregelen,” *Wettelijke Onderzoekstaken Natuur & Milieu,* vol. 114, 2008.

[28] N. Schrieken, A. Gittenberger, J. W. P. Coolen and W. Lengkeek, “Marine fauna of hard substrata of the Cleaver Bank and Dogger Bank,” *Nederlandse Faunistische Mededelingen,* vol. 41, pp. 69-78, 2013.

[29] E. Hammerstedt, “EM technical note: backscattering and seabed image reflectivity 1-5,” 2000.

[30] R. L. Folk, “The distinction between grain size and mineral composition in sedimentary-rock nomenclature,” *J Geol,* vol. 62, no. 4, pp. 344-359, 1954.

[31] EMODnet, “http://www.emodnet-hydrography.eu/,” European Marine Observation and Data Network, 2016. [Online]. [Accessed 5 August 2016].

[32] A. R. Amiri-Simkooei, M. Snellen and D. G. Simons, “Riverbed sediment classification using multi-beam echo-sounder backscatter data,” *J. Acoust.,* vol. 126, pp. 1724-1738, 2009.

[33] K. Pearson, “On lines and planes of closet fit to systems of points in space,” *Philos. Mag.,* vol. 2, no. 6, pp. 559-572, 1901.

[34] H. Hotelling, “Analysis of a complex of statistical variables into principal components,” *J. Educ. Psychol.,* vol. 24, no. 7, pp. 498-520, 1933.

[35] P. R. Bevington and D. K. Robinson, Data Reduction and Error Analysis for the Physical Sciences 3rd edition, New York: McGraw-Hill, 2003.

[36] Siswadi, A. Muslim and T. Bakhtiar, “Variable selection using principal component and procrustes analyses and ITS application in educational data,” *Journal of Asian Scientific Research,* vol. 2, no. 12, pp. 856-865, 2012.

[37] M. J. Canty, Image Analysis, Classification and Change Detection in Remote Sensing with Algorithms for ENVI/IDL, Boca Raton: CRC Press, Taylor & Francis Group, 2007.

[38] R. Tibshirani, G. Walther and T. Hastie, “Estimating the number of clusters in a data set via the gab statistic,” *J. R. Statist. Soc. B,* vol. 63, pp. 411-423, 2001.

[39] L. Kaufman and P. Rousseeuw, Findings Groups in Data: an Introduction to Cluster Analysis, New York: Wiley, 1990.

[40] D. Davies and D. Bouldin, “A cluster seperation measure,” *IEEE Transactions on Pattern Analysis and Machine Intelligence,* Vols. PAMI-1, no. 2, pp. 224-227, 1979.

[41] X. Lurton, An Introduction to Underwater Acoustics, Heidelberg: Springer-Verlag, 2010.

[42] J. M. Preston, A. C. Christney, S. F. Bloomer and I. L. Beaudet, “Seabed Classification of Multibeam Sonar Images,” in *MTS/IEEE Oceans 2001 Conference*, Honolulu, HI, 2001.

[43] A. N. Gavrilov and I. M. Parnum, “Fluctuations of Seafloor Bakscatter Data From Multibeam Sonar systems,” *IEEE Journal of Oceanic Engineering,* vol. 35, no. 2, pp. 209-219, 2010.

[44] E. Jakeman and P. N. Pusey, “Significance of K distributions in scattering elements,” *Physical Review Letters,* vol. 40, no. 9, pp. 546-550, 1978.

[45] L. Hellequin, J. M. Boucher and X. Lurton, “Processing of high-frequency multibeam echo sounder data for seafloor characerization,” *IEEE Journal of Oceanic Engineering,* vol. 28, no. 1, pp. 78-89, 2003.

[46] T. F. Sutherland, J. Galloway, R. Loschiavo, C. D. Levings and R. Hare, “Calibration techniques and sampling resolution requirements for groundtruthing multi-beam acoustic backscatter (EM3000) and QTC VIEW classification technology,” *Estuarine Coastel and Shelf Science,* vol. 75, pp. 447-458, 2007.

[47] E. Alevizos, T. Schoenning, K. Koeser, M. Snellen and J. Greinert, “Quantifying the fine-scale distribution of Mn-nodules: insights from AUV multi-beam and imagery data fusion,” *Currently in press,* 2017.

663

664